(b) For angles $\theta > \pi/2$ the cross section does not vary as rapidly, and at the limit $\theta \approx \pi$ it has the value $d\sigma/d\Omega = k = 1.2 \times 10^{-24}$ cm². Precise measurements at these large angles reveal deviations from the Rutherford equation and are due to the strong interaction (nuclear interaction, see Table 6.1) between the alpha particle and the gold nucleus.

As explained in detail in the introduction to this chapter, the nuclear interaction will manifest itself only at short distances—that is, at high-momentum transfers q (Eq. 1.4), where $q = 2p \sin \theta/2$. Clearly the maximum momentum transfer in this experiment is

$$q = 2p = 2\sqrt{2Em} = 200 \text{ MeV}/c$$

The recent experiments on Coulomb scattering of electrons from protons have been extended to $q \simeq 2.2$ BeV/c.

3. Compton Scattering

3.1 Frequency Shift and Cross Section

This section deals with the scattering of electromagnetic radiation by free electrons. As mentioned in the introduction to this chapter, it is the scattering of electromagnetic radiation from various objects that makes it possible for us to "see" them. However, as the frequency of the radiation is increased beyond the visible region, the light quanta have energies comparable to, or larger than the binding energy of the electrons in atoms, and the electrons can therefore be considered as free.

In 1920 A. H. Compton investigated the scattering of monochromatic x-rays from various materials. He observed that after the scattering, the energy (frequency) of the x-rays had changed, and had always decreased. From the point of view of classical electromagnetic theory, this frequency shift cannot be explained,† since the frequency is a property of the incoming electromagnetic wave (field) and cannot be altered by the change of direction implied by the scattering. If, on the other hand, we think of the incoming radiation as being represented by a beam of photons, we need only consider the scattering of a quantum of energy $E = h\nu$ from a free electron; then, because of energy-momentum conservation, the scattered quantum has energy $E' = h\nu' < E$, in complete agreement with the experiments of Compton.

The frequency shift will depend on the angle of scattering and can be easily calculated from the kinematics. Consider an incoming photon of energy $E = h\nu$ and momentum $p = h\nu/c$ (Fig. 6.8) scattering from an electron of mass m; $\mathbf{p}$ is the momentum of the electron after scattering and

† See, for example, J. D. Jackson, *Classical Electrodynamics*, John Wiley, p. 488.

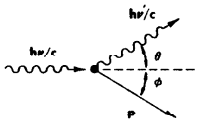

FIG. 6.8 Compton scattering of a photon from a free electron.

$h\nu'$, $\mathbf{h}\nu'/c$ the energy and momentum of the photon after the scattering. The three vectors $\mathbf{h}\nu/c$, $\mathbf{h}\nu'/c$, and $\mathbf{p}$ must lie on the same plane, and energy conservation yields

$$h\nu + mc^2 = h\nu' + \sqrt{p^2c^2 + m^2c^4} \tag{3.1}$$

From momentum conservation we obtain

$$h\nu = h\nu' \cos\theta + cp \cos\phi \tag{3.2}$$

$$0 = h\nu' \sin\theta + cp \sin\phi \tag{3.3}$$

Here θ is the photon scattering angle, and ϕ the electron recoil angle. To solve the above equations we transpose appropriately, square, and add Eq. 3.2 and Eq. 3.3 to obtain

$$h^2\nu^2 - 2h^2\nu\nu' \cos\theta + h^2\nu'^2 = c^2p^2$$

while by squaring Eq. 3.1,

$$h^2\nu^2 + h^2\nu'^2 - 2h^2\nu\nu' + 2hmc^2(\nu - \nu') = c^2p^2$$

which by subtraction yields

$$\frac{\nu - \nu'}{\nu\nu'} = \frac{h}{mc^2}(1 - \cos\theta) \tag{3.4}$$

We can recast Eq. 3.4 into two more familiar forms: (a) to give the shift in wavelength of the scattered x-ray beam:

$$\Delta\lambda = \lambda' - \lambda = \frac{h}{mc}(1 - \cos\theta) \tag{3.5}$$

or (b) to give the energy of the scattered photon:

$$E' = \frac{E}{1 + (E/mc^2)(1 - \cos\theta)} \tag{3.6}$$

From Eq. 3.5 we see that the shift in wavelength, except for the angular

dependence, is a constant, the Compton wavelength†

$$h/mc = 2.42 \times 10^{-10}\ \text{cm} = 0.0242\ \text{Å}$$

For low-energy photons, with $\lambda \gg 0.02$ Å, the Compton shift is very small, whereas for high-energy photons with $\lambda \ll 0.02$ Å, the wavelength of the *scattered* radiation is always of the order of 0.02 Å, the Compton wavelength. These conclusions can equally well be obtained from Eq. 3.6, where the energy shift increases when E/mc^2 becomes large. For $E/mc^2 \gg 1$, E' is independent of E and of the order $E' \approx mc^2$. [Hence $\lambda' = c/\nu' = c/(E'/h) \simeq c/(mc^2/h) = h/mc$ as stated before.]

As an example, in this laboratory gamma rays from Cs^{137} are scattered from an aluminum target; since $E = 0.662$ MeV, we have $E/mc^2 = 1.29$, so that back-scattered gamma rays ($\theta = 180°$) will have $E' = E/3.6$, which is less than 30 percent of their original energy. It thus becomes quite easy to observe the Compton energy shift as compared to x-ray scattering, where, if we assume $\lambda = 2$ Å, $\Delta\lambda/\lambda = \Delta E/E = 0.01$.

In the original experiments Compton and his collaborators observed (especially for high Z materials) in addition to the frequency shifted x-rays, scattered radiation *not shifted* in frequency. The unshifted x-rays are due to scattering from electrons that remained bound in the atom‡: in this process the recoiling system is the entire atom, and we replace in Eq. 3.5 m by m_A (where $m_A \simeq 2{,}000 \times A \times m_e$) resulting in an undetectable wavelength shift, $\Delta\lambda' \approx 10^{-7}$ Å.

Next we are interested in the differential cross section for the scattering of the radiation from the electrons. Classically this is given by the Thomson cross section,§ which can be easily derived: consider a plane wave propagating in the z direction with the E vector linearly polarized along the x direction. This is incident on an electron of mass m, as shown in Fig. 6.9 The electron will experience a force $F = eE = eE_0 \cos \omega t$, and its acceleration will be

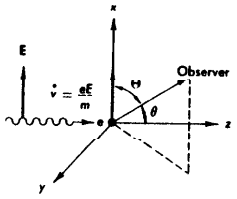

FIG. 6.9 Classical picture of the scattering of electromagnetic radiation by an electron; this leads to the Thomson cross section.

$$\dot{v} = \frac{eE_0}{m} \cos \omega t$$

† The mass of the electron m_e was used in evaluating h/mc; by using the mass of the pion, or other particle, we obtain the pion Compton wavelength, and so forth.

‡ A similar situation is discussed in the following section on the Mössbauer effect, where the nucleus remains bound in the lattice and the recoiling system is the entire crystal.

§ Already discussed in Chapter 5, Section 2.5.

According to Eq. 2.26, Chapter 5, the power radiated by this accelerated electron will be (nonrelativistically, in MKS units)

$$\frac{dP}{d\Omega} = \frac{e^2}{(4\pi\epsilon_0)^2 \mu_0 c^5} \dot{v}^2 \sin^2 \Theta \tag{3.7}$$

where Θ is the angle between the direction of observation and the E vector of the incoming wave. Using the expression for $\dot{v}$, we can write for Eq. 3.7 averaged over one cycle

$$\left\langle \frac{dP}{d\Omega} \right\rangle = \frac{1}{2} \left(\frac{e^2}{4\pi\epsilon_0 mc^2} \right)^2 \epsilon_0 E_0^2 c \sin^2 \Theta$$

Finally, from the definition for a cross section given in Chapter 5, Section 2.1, we have

$$\frac{d\sigma}{d\Omega} = \frac{\text{energy radiated/(unit time-unit solid angle)}}{\text{incident energy/(unit area-unit time)}}$$

Here the denominator is clearly given by the Poynting vector

$$\langle P \rangle = \frac{1}{2} \sqrt{\frac{\epsilon_0}{\mu_0}}\, E_0^2 = \tfrac{1}{2} \epsilon_0 c E_0^2$$

Thus we obtain

$$\frac{d\sigma}{d\Omega} = \left(\frac{e^2}{4\pi\epsilon_0 mc^2} \right)^2 \sin^2 \Theta \tag{3.8}$$

Where

$$\frac{e^2}{4\pi\epsilon_0 mc^2} = r_0$$

has dimensions of length, the so-called "classical electron radius"

$$r_0 = 2.82 \times 10^{-15}\ \text{cm}$$

Finally, we average over all possible directions of polarization of the incoming wave and use the angle θ measured from the direction of propagation of the wave to obtain

$$\frac{d\sigma}{d\Omega} = r_0^2 \left(\frac{1 + \cos^2 \theta}{2} \right) \text{cm}^2 \tag{3.9}$$

When integrated over all angles, Eq. 3.9 yields the Thomson cross section

$$\sigma_T = \frac{8\pi}{3} r_0^2 \tag{3.10}$$

(also given in Chapter 5, Eq. 2.19).

Several objections can be raised to the simple cross section given by Eq. 3.9 or Eq. 3.10: (a) it does not depend on frequency, a fact not supported by experiment; (b) the electron, even though free, is assumed not to recoil; (c) the treatment is nonrelativistic; and (d) quantum effects are not taken into account. Indeed, the correct quantum-mechanical calculation for Compton scattering yields the so called Klein-Nishina formula†

$$\frac{d\sigma}{d\Omega} = r_0^2 \frac{1 + \cos^2\theta}{2} \frac{1}{[1 + \gamma(1 - \cos\theta)]^2} \times \left[1 + \frac{\gamma^2(1 - \cos\theta)^2}{(1 + \cos^2\theta)[1 + \gamma(1 - \cos\theta)]}\right] \quad (3.11)$$

where r_0 and θ were defined previously, and $\gamma = h\nu/mc^2$. The cross section has been averaged over all incoming polarizations. By integrating Eq. 3.11, the total cross section can be had. We will not give the complete result here, but the assymptotic expressions have already been presented in Chapter 5, Eq. 2.21.

A comparison of the Thomson (Eq. 3.9) and Klein-Nishina cross sections, including the results obtained in this laboratory for $\gamma = 1.29$, is shown in Fig. 6.14. We remark that although the Thomson cross section is symmetric about 90°, the Klein–Nishina cross section is peaked forward strongly as γ increases. This is due to a great extent to kinematical factors associated with the Lorentz transformation from the center of mass to the laboratory; note that the center of mass velocity of the (quantum + free electron) system is

$$v = \beta c = c\gamma/(1 + \gamma)$$

where as before $\gamma = h\nu/mc^2$.

The experimental data are in perfect agreement with the results of Eqs. 3.6 and 3.11, which are among the most impressive and convincing successes of quantum theory. In the following two sections we will describe the experimental verification of these predictions.

3.2 The Compton Scattering Experiment

As with any scattering experiment, the apparatus will consist of:

(a) The beam of incident particles, in this case photons.
(b) The target (containing the electrons from which the photons scatter).
(c) The detector of the scattered photons.

† See W. Heitler, *The Quantum Theory of Radiation*, 3rd ed., Oxford University Press, p. 219.

The beam of photons is obtained by collimating the gamma radiation from a Cs^{137} source. As we know (Table 4.2) Cs^{137} (Ba^{137}) emits a gamma ray of energy 0.662 MeV, and the detection techniques have been discussed in Chapter 5. In Fig. 5.28 is shown the pulse-height spectrum of the gamma radiation from Cs^{137}, as obtained with standard equipment; the same detection equipment is used in this experiment with the only difference that the scintillation crystal is placed in a heavy shield.

A schematic of the apparatus is shown in Fig. 6.10. The lead pig *A* is fixed and holds the source, which can be introduced through the vertical hole (v). Another lead shield *B* contains the detector and can be rotated about the center, where the target is located. The lead assemblies are rather heavy (approximately 200 lb) and some provisions must be taken for adequate mounting.

For the source, a 35-mCi Cs^{137} sample was used, which was properly encapsulated before being shipped to the laboratory. It should always be transported in a lead container, and when transferred into the lead pig *A*, it must be handled only by the attached string. The source holder (*A*) has a collimator (*h*) drilled horizontally, subtending a solid angle of the order of 0.03 sr. Of interest to us will be the density of the photon beam at the target, and the *expected* value is

$$\frac{3.7 \times 10^{10} \times 0.035}{4\pi} \frac{1}{r^2} = 8.8 \times 10^4 \text{ photons/cm}^2\text{-sec}$$

Where we use $r = (13.5 \times 2.54) = 34.3$ cm, as read off Fig. 6.10; indeed the observed density of 41×10^2 photon/cm²-sec is of the predicted order of magnitude.

In contrast to the situation in Rutherford scattering, there is no need to enclose the beam and detector in vacuum or to use a very thin target. We know that gamma rays do not gradually lose energy when traversing matter as a charged particle does, but their interaction can be characterized by a mean free path. For the Cs^{137} gamma ray we find from Fig. 5.34

$$\lambda = 4.7 \text{ cm in Al}; \quad \lambda = 0.92 \text{ in Pb}$$

this corresponds to 10^4 cm of air, so that the interaction of the photon beam in the air of the apparatus (approximately 100 cm) is indeed negligible. Also, the target thickness can safely be a fraction of a mean free path before the probability for multiple interactions becomes considerable. Aluminum targets ½-in. thick are quite adequate for this experiment.

Some special mention must be made of the geometrical shape of the target. We may use a flat target (such as an aluminum plate), in which event the cross section is obtained by considering the interaction of the total beam with the number of electrons per square centimeter of the

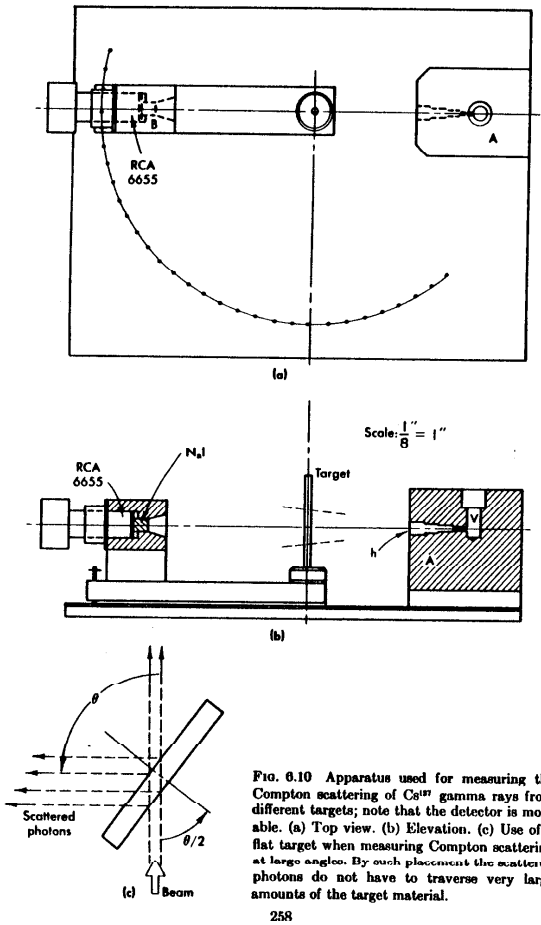

FIG. 6.10 Apparatus used for measuring the Compton scattering of Cs^{137} gamma rays from different targets; note that the detector is movable. (a) Top view. (b) Elevation. (c) Use of a flat target when measuring Compton scattering at large angles. By such placement the scattered photons do not have to traverse very large amounts of the target material.

target†; alternatively, we may use a target of circular cross section (such as a rod), in which event the cross section is obtained by considering the interaction of the beam density (photons per square centimeter) with the total number of electrons in the target.† When using a plate, it is advisable to rotate it so that it always bisects the angle between beam and detector, since otherwise the scattered photons may have to traverse a very large amount of material before leaving the target (see Fig. 6.10c). In that case, however, the amount of scattering material in the beam path varies as $1/\cos(\theta/2)$, and this correction must be applied to the yield of scattered particles. These effects are obviously eliminated when a target of circular cross section is used. In addition, the scattering point is better defined even if the beam is only poorly collimated. On the other hand, accurate evaluation of the flux density at the target is difficult. The results presented here were obtained by using a $\frac{1}{2}$-in. aluminum rod as the target.

An interesting refinement of the technique is made by observing the recoil electrons in time coincidence with the scattered photon. However, the kinetic energy of the recoil electron is

$$T_e = E - E' = E\frac{\gamma(1 - \cos\theta')}{1 + \gamma(1 - \cos\theta)}$$

which at its maximum value ($\theta = 180°$) is

$$T\text{ (electron)} = 0.662 \times (2.58/3.58) = 475\text{ keV}$$

The range of such an electron in aluminum is only 150 mg/cm² (see, for example, Feather's rule, Chapter 5, Eq. 2.13), which corresponds to approximately 0.06 cm. Thus, the recoil electrons will, in almost all cases, stop in the target. On the other hand, if a plastic scintillator is used as the target, and is viewed with a photomultiplier, the recoil electrons do produce a signal that can be easily detected.

As mentioned before, the detection system consisted of a NaI crystal mounted on a 6655 RCA photomultiplier. The dimensions of the crystal were 1-in. diameter and 1-in. thick. In Fig. 6.11 are shown two typical pulse-height spectra: one at 0° which obviously is dominated by the primary beam and does not change whether the target is in place or removed; and one at 120°, where the photopeak is again clearly observable but appears at a much lower discriminator setting.

By measuring the pulse-height distribution at various angles, we obtain the energy of the scattered photons as it is given by the position of the photopeak, and under the assumption that the discriminator is linear (see Fig. 5.31). To obtain the yield of scattered photons, we may either (a) accept all counts above noise level and apply a correction for the efficiency

† See Fig. 5.1.

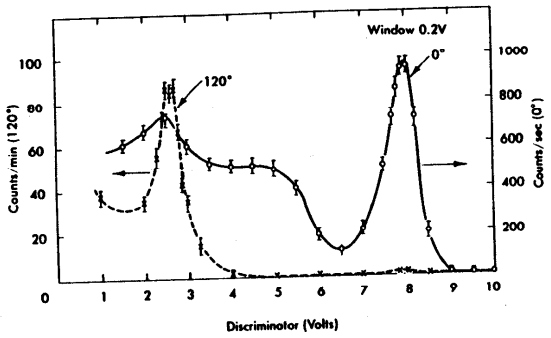

FIG. 6.11 Pulse-height spectrum of scattered gamma rays, at 0° (solid curve) and at 120° dotted curve; note the shift of the photopeak indicating a shift in the energy of the incident gammas.

of the crystal, or (b) integrate the counts in the photopeak only and apply a correction for the "photofraction" as well as for crystal efficiency. These corrections depend on the crystal size and on the photon energy (which varies with angle); Fig. 6.12 gives the efficiency against energy for a 1-in. diameter, 1-in. thick NaI crystal.† In the present experiment we have chosen the former method, that is, of accepting all counts above noise level.

In this experiment, unlike the Rutherford scattering experiment the background is quite low. When the detector is moved outside the primary beam, which has an angular width of $\theta_0 \approx 8°.5$, the background counts are less than 0.01 of the scattered counts. Further, the cross section for Compton scattering falls off much more slowly than $1/(\sin^4\theta/2)$, and therefore a higher background can be tolerated; thus useful data can be obtained at large angles. We also note that Cs^{137} emits mainly the 0.662-MeV gamma ray and 0.514-MeV electrons; these electrons, however, can hardly penetrate the target, much less reach the detector.

3.3 Results and Discussion

The results presented below were obtained by students‡ using the apparatus described in the previous section.

† From *Scintillation Phosphors*, Harshaw Chemical Company, Cleveland, Ohio.

‡ D. Kohler and A. Rosen, class of 1962.

At first the beam is surveyed by measuring the profile (see Section 2.3 on Rutherford scattering) and it is ascertained that the pulse-height spectrum has the correct shape, as shown in Fig. 6.11. The beam is found to have an angular spread† of $\theta_0 = \pm 8°.5$, consistent with the dimensions of the source collimator; from Fig. 6.10 we find $\tan\theta_0 = 1.5/13.5 = 0.110$, thus $\theta_0 \approx 7°$. The peak beam-rate, which is fairly flat near the center is 25.4×10^3 counts/sec, which corresponds to a density at the detector of

$$\text{flux} = 5 \times 10^2 \text{ counts/cm}^2\text{-sec}$$

We have to correct this rate for the efficiency of the crystal, which at this energy (Fig. 6.12) is $\epsilon = 0.47$, and to extrapolate from the density at the detector to the flux density at the target. Assuming a $1/r^2$ dependence and since r (source detector) $= 2r'$ (source-target) as shown in Fig. 6.10, we obtain

$$\text{flux (at target)} = \frac{5 \times 10^2}{\epsilon} \times \left(\frac{r}{r'}\right)^2 = 42.6 \times 10^2 \text{ photons/cm}^2\text{-sec}$$

Next, a pulse-height spectrum is taken at different angles and the position of the photopeak carefully measured. Two such spectra have already been shown in Fig. 6.11; these were taken with a discriminator window 0.2 V wide (the abscissa is calibrated in volts). To avoid drifts of the detection system, after each pulse-height spectrum is taken, the detector as-

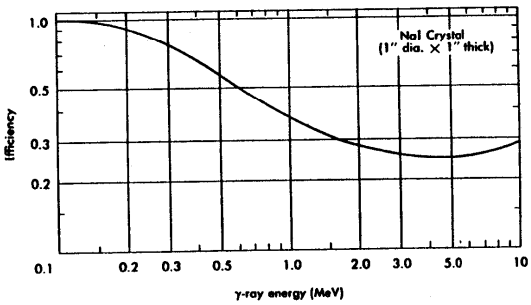

FIG. 6.12 Efficiency of a NaI crystal for the detection of gamma rays, as a function of their energy.

† Full width at half maximum, 17°.

TABLE 6.3
PHOTOPEAK POSITION AS A FUNCTION OF ANGLE

Angle (degrees)	Discriminator channel	Energy	$(1 - \cos\theta)$
0	7.95	0.662	0
20	7.45	0.620	0.06
50	5.45	0.455	0.36
60	4.80	0.400	0.50
70	4.30	0.358	0.66
90	3.45	0.287	1.00
120	2.60	0.218	1.50

sembly is returned to 0° and the center of the photopeak is scanned. The photopeak values are summarized in the following Table 6.3 and are also shown in Fig. 6.13. We plot the inverse of the photon energy, $1/E'$, against

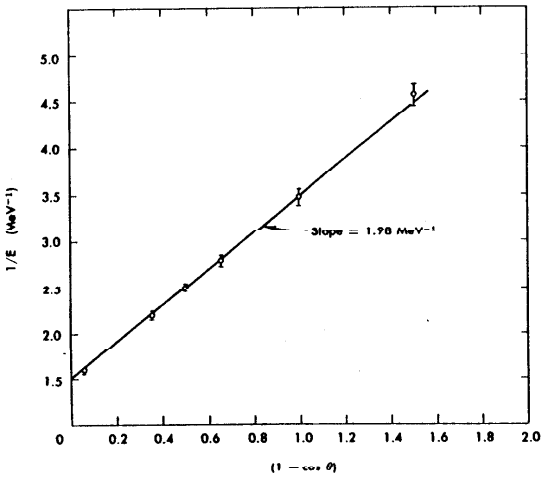

FIG. 6.13 The results obtained for the energy (frequency shift) of the Compton scattered gamma rays. Note that $1/E$ is plotted against $(1 - \cos\theta)$ leading to a linear dependence; the slope of the line gives the mass of the electron

TABLE 6.4
DIFFERENTIAL CROSS SECTION FOR COMPTON SCATTERING

Angle (degrees) (1)	E (MeV) (2)	Yield (counts/sec) (3)	Efficiency ϵ (4)	Corrected yield (5)	$d\sigma/d\Omega$ (experimental) (6)	Klein-Nishina (7)
					$\times 10^{-26}$ cm²	$\times 10^{-26}$ cm²
0	0.662					6.65
20	0.614	52.2	0.47	111.0	6.06	5.39
30	0.564	35.1	0.49	71.5	3.90	4.29
40	0.503	27.5	0.52	51.0	2.78	3.19
50	0.452	20.7	0.55	37.7	2.06	2.42
60	0.402	17.7	0.60	29.5	1.61	1.85
70	0.353	15.3	0.65	23.5	1.28	1.50
80	0.320	13.7	0.69	20.0	1.09	1.23
90	0.289	13.6	0.72	19.0	1.04	1.09
100	0.263	12.5	0.75	16.6	0.91	1.02
110	0.242	13.4	0.78	17.2	0.94	1.01
120	0.225	14.8	0.81	18.3	1.00	0.97
130	0.211	14.8	0.84	17.6	0.96	0.97
140	0.201	16.6	0.86	19.3	1.05	0.99
150	0.193	17.1	0.88	19.4	1.06	0.98

$(1 - \cos\theta)$; according to Eq. 3.6, a straight line should be obtained, since

$$\frac{1}{E'} - \frac{1}{E} = \frac{1}{mc^2}(1 - \cos\theta)$$

This is indeed the result, and the slope of the line gives $1/mc^2$; from a least-squares fit we obtain

$$mc^2 = 505 \pm 12 \text{ keV}$$

in very good agreement with the known value of the electron mass.

We thus conclude that Eq. 3.6 is very well verified and that our explanation of the Compton frequency shift is firmly supported by these data.

We next turn to the evaluation of the differential cross section. As explained before, all counts above the 1 V level were accepted, and data were taken at several angles. The results are summarized in Table 6.4: here column 1 gives the angle and column 2 the corresponding photon energy; column 3 gives the raw yield in counts per second at that particular angle; column 4 gives the efficiency of the detector for the photon energy (of column 2) as obtained from Fig. 6.12, and the corrected counting rate appears in column 5.

To obtain the cross section we note that

$$\frac{d\sigma}{d\Omega} = \frac{\text{yield}}{(d\Omega)NI_0}$$

From Fig. 6.10 we see that the detector solid angle is given by

$$d\Omega = \frac{\text{crystal area}}{r^2} = \frac{5.07\ \text{cm}^2}{(34.3)^2\ \text{cm}^2} = 4.3 \times 10^{-3}\ \text{sr}$$

For the total number of electrons in the target, we have

$$N = \pi\left(\frac{d}{2}\right)^2 h\rho\frac{N_0}{A}Z$$

Where

d = diameter of target = 1.27 cm
h = height of target† = 10 ± 2 cm
ρ = density of aluminum = 2.7 gm/cm³
N_0 = Avogadro's number = 6×10^{23}
A = atomic weight of aluminum = 27
Z = atomic number of aluminum = 13

thus

$$N = 10^{25}\ \text{electrons}$$

For I_0, the flux density at the target, we use the previously obtained value

$$I_0 = 42.6 \times 10^3\ \text{photons/cm}^2\text{-sec}$$

so that finally

$$\frac{d\sigma}{d\Omega} = \frac{\text{corrected yield}}{4.3 \times 10^{-3} \times 10^{25} \times 42.6 \times 10^3} = \frac{\text{corrected yield}}{1.83 \times 10^{27}}$$

The values of the differential cross section obtained in this fashion are given in column 6 of Table 6.4, and are also plotted in Fig. 6.14. The solid line in Fig. 6.14 gives the theoretical values for $d\sigma/d\Omega$ derived from the Klein–Nishina formula (Eq. 3.11) for $\gamma = 1.29$, while the dashed curve represents the Thomson cross section.

The agreement of the *angular dependence* of the experimental points with the theoretical curve is indeed quite good and clearly indicates the inadequacy of the Thomson cross section for the description of the scattering of high-energy photons, while confirming the Klein–Nishina formula. On the other hand the *absolute value* of the experimental cross section is subject to considerable error due to the way in which the flux density I_0 and total number of electrons N were estimated. Therefore, in spite of the close agreement of the absolute values of the experimental data with the theoretical curve, we may only conclude that the observed cross section is of the correct order of magnitude.

† This is obtained by estimating the length of target intercepted by the beam. We assume that the angular spread in the vertical direction is the same as in the horizontal, $\phi_0 = \pm 2°5$ and use $r = 34.3$ cm; see also Fig. 6.10.

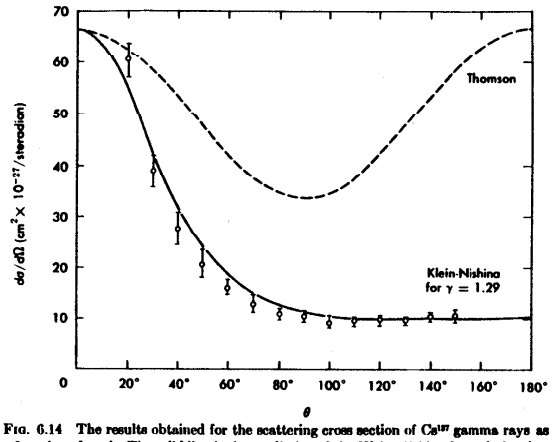

FIG. 6.14 The results obtained for the scattering cross section of Cs^{137} gamma rays as a function of angle. The solid line is the prediction of the Klein-Nishina formula for that particular energy; the dotted line is the Thomson cross section.

4. Mössbauer Effect

4.1 General Considerations

In the two experiments previously described, we could visualize the scattering process as if it were a collision of two billiard balls in which the incoming alpha particle or photon maintained its identity but suffered a change in momentum and energy. The phenomenon of scattering can, however, also be visualized as the absorption by the target of quanta of the incoming beam, with the subsequent re-emission of these quanta; this was the model we used in the derivation of the Thomson scattering cross section in the previous chapter.